Yossef, Mostafa; Noureldin, Mohamed; Al Kabbani, Aghyad

Explainable artificial intelligence framework for FRP composites design

Published in:
Composite Structures

DOI:
10.1016/j.compstruct.2024.118190

Published: 01/08/2024

Document Version
Publisher's PDF, also known as Version of record

Composite Structures 341 (2024) 118190

Contents lists available at ScienceDirect

Composite Structures

journal homepage: www.elsevier.com/locate/compstruct

Explainable artificial intelligence framework for FRP composites design

Mostafa Yossef [a,b], Mohamed Noureldin [a,*], Aghyad Alqabbany [a]

[a] Aalto University, Espoo, Finland
[b] Arab Academy for Science, Technology and Maritime Transport, Cairo, Egypt

ARTICLE INFO

Keywords:
Composite design
FRP
Explainable artificial intelligence
Machine Learning
Counterfactual
Casual AI
SHapley Additive exPlanations
Partial Dependence Plots

ABSTRACT

Fiber-reinforced polymer (FRP) materials are integral to various industries, from automotive and aerospace to infrastructure and construction. While FRP composite design guidelines have been established, the process of obtaining the desired strength of an FRP composite demands considerable time and resources. Despite recent advancements in Machine Learning (ML) models which are commonly used as predictive models, the inherent 'black box' nature of those models poses challenges in understanding the relationship between input design parameters and output strength of the composite. Moreover, these models do not provide tools to facilitate the designing process of the composite. The current study introduces an explainable Artificial Intelligence (XAI) framework that will provide understanding for the input–output relationships of the model through SHapley Additive exPlanations (SHAP) and Partial Dependence Plots (PDPs). In addition, the framework provides for the first time a designing approach for adjusting the important design parameters to obtain the desired composite strength by the designer through utilizing an explainability technique called Counterfactual (CF). The framework is evaluated through the design of a 14-ply composite, successfully identifying critical design parameters, and specifying necessary adjustments to meet strength requirements.

1. Introduction

Fiber-reinforced polymer (FRP) materials have gained attention in the last few decades due to their high strength, non-corrosive behavior, and easy manufacturing. FRP materials are essential to many industries, including automotive, aerospace, and construction industries. Design for FRP composites has been developed through the years to include all size aspects (Fig. 1), starting from microscale, which includes ply behavior and the interaction between fiber and the surrounding matrix, then mesoscale, which is focused on the interaction between different laminas, and finally with the composite structure scale which is applied for structures such as sandwich panels [1–5], wind blades [6–8], and marine structures [9–11]. To achieve certain strengths, designers have to choose between selective materials, lamina orientation, and layer arrangement to come up with the best possible combination.

With the growing number of materials and unlimited configuration possibilities, the need for automated processes is growing more than ever. Researchers developed optimization tools to automate the design process such as Genetic Algorisms (GA) [13,14]. However, using optimization tools such as GA is not practical for everyday design use since it has high computational cost and can sometimes results in local optimization results which can be considered time consuming for designers.

In recent years, Machine Learning (ML) models have emerged as powerful tools in many engineering fields and applications [15–20] such as design and characterization of microstructures of materials [21–23], carbon nanotube composites [24,25], and resilient structures [26–29]. These models are trained on a subset of available data to make accurate predictions for the required output response quantity. They serve as efficient alternatives to traditional methods like experimental testing and Finite Element (FE) analysis, offering substantial time and cost savings. The efficacy of ML models is typically evaluated based on their accuracy in predicting the behavior under study.

The implementation of ML in composites has been boosted in the last decade [30–32]. For example, a ML model using a genetic algorithm (GA) and optimized back propagation (BP) neural network are used to predict the transverse mechanical properties considering micro voids between fibers and matrix [33]. Artificial neural network (ANN) and particle swarm optimization (PSO) are applied to estimate the relationship between input parameters, including the thermal conductivity of fiber and matrix and volume fraction, and the thermal conductivity of the composite as an output parameter [34]. ANN is the one of the

* Corresponding author.
E-mail address: mohamed.noureldin@aalto.fi (M. Noureldin).

https://doi.org/10.1016/j.compstruct.2024.118190
Received 22 November 2023; Received in revised form 21 April 2024; Accepted 5 May 2024
Available online 7 May 2024

commonly used ML models for constitutive modeling of composite materials [35,36].

The prediction of laminate behavior in the mesoscale is carried out by using different ML algorithms, including convolutional neural networks (CNN) [37,38], minimax probability machine regression (MPMR), and multivariate adaptive regression spline (MARS) [39], XGBoost, Random Forests, Gaussian Processes and Artificial Neural Networks [40]. A combination of ANN and analytical models are used to predict the shear modulus (G_{12}) and longitudinal ultimate tensile strength (X_T) of unidirectional composites [41]. Lui et al proposed a framework based on XGBoost to study the pultruded FRP composites exposed to water and humidity [42]. XGBoost has recently gained attention due its excellent capabilities of solving nonlinear regression problems, thus providing a high level of accuracy compared to other models [43]. Recent advances in composites using ML models are listed in detail in the literature [32,44].

Most of the applied machine learning models [45,46] are used for the prediction of the ply and laminate behavior (by using fixed input parameter values) rather than being used as a design tool (by changing the input parameters) for obtaining the required output (for example, strength). The designer's grasp of the relationship between input material parameters and output strength is paramount. Traditional ML models, often viewed as 'black boxes', fall short in providing this critical insight and lack interpretability. This is where the advent of explainable AI (XAI) tools [45,47,48] steps in, prioritizing interpretability. These tools bridge the gap, offering designers a clearer understanding of how input factors influence output responses, empowering them to make more informed decisions in the design process. For example, an Explainable AI (XAI) approach employing the SHapley Additive exPlanations (SHAP) model has been applied to investigate the significance of material properties, geometrical dimensions, and environmental factors in bistable composite laminates [49]. The findings highlight that the transverse thermal expansion coefficient and moisture variation exert the most significant influence on the transverse curvature. In recent studies, XAI has been utilized to gain insight into the behavior of composites with edge cracks [50]. Additionally, researchers have acknowledged SHAP as a valuable method for examining crucial parameters in composites subjected to impact [51]. Beyond composites, XAI has found widespread application in comprehending the role of input parameters in various structural contexts [52–54].

Despite the aforementioned studies show the capability of the XAI in understanding the role of input features and their effect on the overall output, they fall short in actively manipulating these features to attain a desired output response. In other words, the previous studies merely use XAI technique as a descriptive approach for revealing the input–output parameters relationship without offering a systematic approach to adjust inputs for achieving the necessary output, which is important for the composite design process. In the current study, a novel XAI framework is introduced using SHapley Additive exPlanations (SHAP), Partial Dependence Plots (PDPs), and Counterfactual (CF) concepts to provide a design tool for FRP composites. The framework highlights the crucial design input parameters and then provide a strategy for finetuning those parameters to achieve the required strength of the composite.

2. The proposed framework

This study proposes an explainable ML framework that can help designers understand the most influential input parameter and its relationship with the desired strength parameter. In addition, it allows the designer to control main design parameters to achieve the required strength of the composites. The framework is based on several assumptions as follows:

1. The laminate consists of 14 plies to increase the number of permutations, where manual design techniques are hard to apply [55].
2. Bending is the main straining action in the longitudinal direction of the laminate, which is assumed as the same direction as the longitudinal modulus (E_1). Therefore, the transverse direction is negligible due to the nature of the application, i.e., bending of the FRP bridge deck panel.
3. Some layers are independent of orientation (chopped mat strands) based on an optimization study of the optimal lamina arrangement conducted for obtaining maximum laminate strength.
4. Symmetric laminate is adopted to avoid warping due to thermal loading.

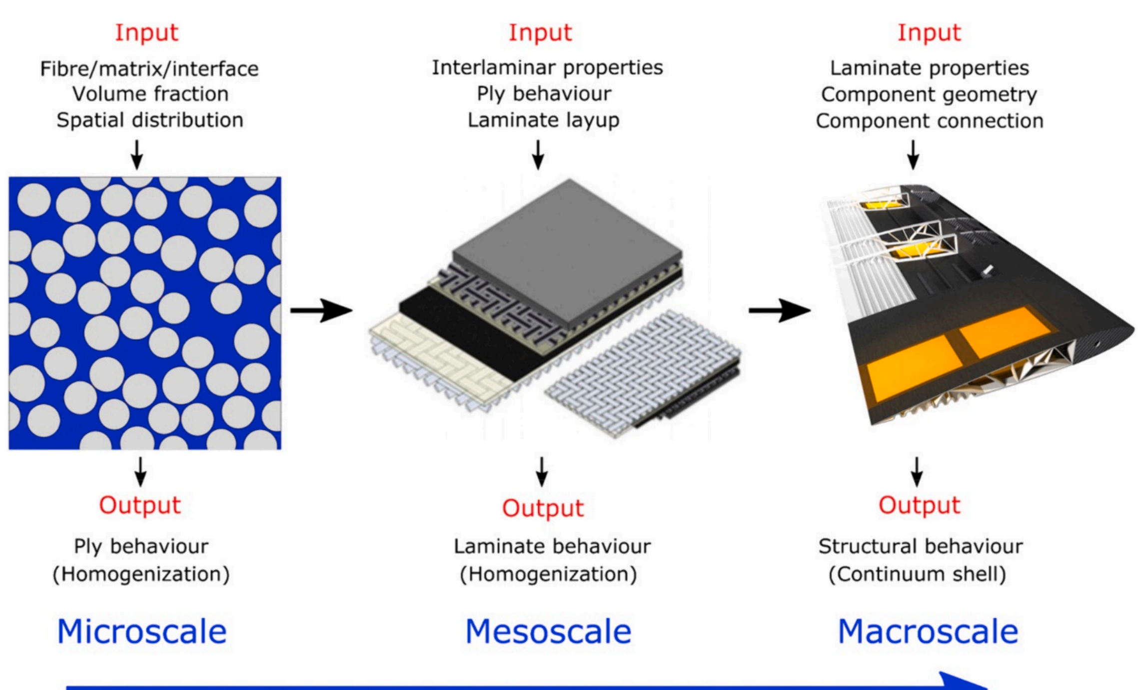

Fig. 1. Schematic of bottom-up multi-scale modeling of engineering composite structures [12].

5. The orientation of the laminate is fixed while the same material is not stacked consecutively to avoid unidirectional laminates and reduce computational cost during optimization.

The stages of the proposed framework are shown in Fig. 2. The framework consists of five main stages: 1. selecting the optimal lamina arrangement, 2. dataset generation using design of experiments and Latin Hypercube Sampling (LHS) technique, 3. machine learning training for predicting composite strength, 4. explainable artificial intelligence (XAI) techniques are modeled to highlight the most important design parameters, and finally 5. the design stage is performed using Counterfactual (CF), where the model chooses the best path to achieve the desired design strength by varying the important design parameters.

The details of each step of the proposed framework are described as follows:

Stage 1, Selecting optimal lamina arrangement:

In this stage, the optimal stacking arrangement is investigated using Brute Force optimization technique, to obtain the maximum possible strength of the composite. Brute Force optimization is a straightforward, exhaustive search method that explores all possible solutions within a defined parameter space. It systematically evaluates each candidate solution to find the one that optimizes the objective function. This is done by discretizing the parameter space into a grid or set of discrete points. Each point represents a potential solution, and the objective function is computed for each of these points. The solution with the highest objective function value (i.e., composite strength) is considered the optimal solution. This method guarantees finding the global optimum within the search space. In each trial, the lamina is stacked in a different arrangement and the corresponding strength of the composite is calculated using a high-performance computer with several cores to

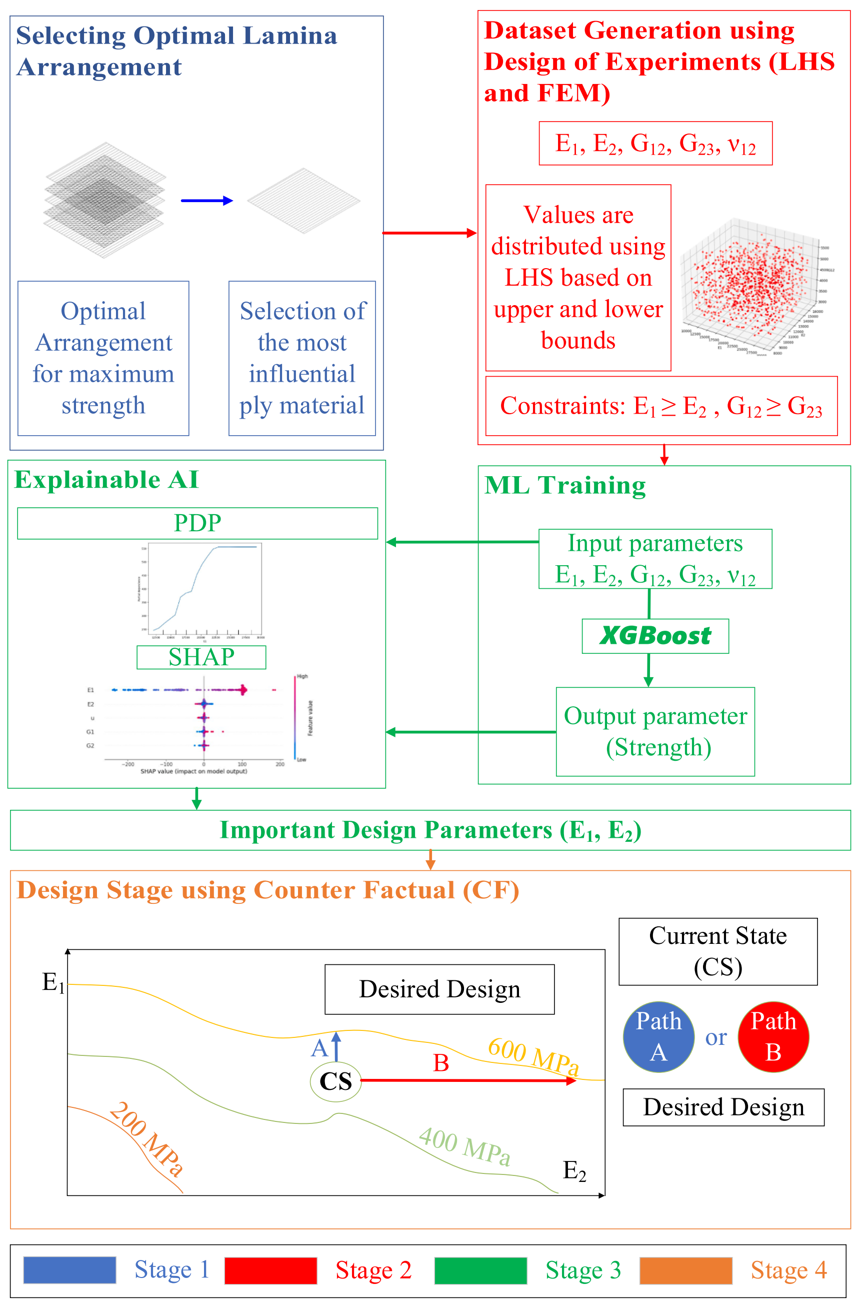

Fig. 2. Schematic diagram showing the proposed framework, E_1 is longitudinal modulus, E_2 is transverse modulus, G_{12} are the shear modulus associated with 12 and 23 planes, respectively, and ν_{12} is Poisson's ratio.

reduce the computational time. After that, the most influential ply material is identified according to the position of the layers. The top and bottom layers are often considered the most influential layers when the laminate is subjected to bending. The configuration is assumed to be symmetric, leading to the same ply material assigned to the top and bottom layers, which is then selected as the most influential ply material.

Stage 2, Dataset generation:

The material characteristics of the dominant lamina are allocated within specified practical upper and lower limits considering for commercially available plies. The studied input parameters (material characteristics, where 1 and 2 defines longitudinal and transverse axes of the ply, respectively) are longitudinal modulus (E_1), transverse modulus (E_2), shear modulus associated with 12 plane (G_{12}), shear modulus associated with 23 plane (G_{23}) and Poisson's ratio (ν_{12}). This allocation ensures that the longitudinal stiffness is greater than or equal to the transverse stiffness (Constraints: $E_1 \geq E_2$, $G_{12} \geq G_{23}$). This is basically related to the use of the composite in engineering applications (e.g., bridge deck) where loading in the longitudinal direction is expected to be the dominant loading condition compared to the transverse direction.

In this present investigation, the Latin Hypercube Sampling (LHS) technique is utilized, which involves the stratification of the probability distribution function of the random variables. These variables are the material characteristics (E_1, E_2, G_{12}, G_{23}, ν_{12}). This approach leads to a notable reduction in the number of required simulations compared to the conventional Monte Carlo simulation method. LHS technique ensures a more efficient and even exploration of the input parameter space by dividing it into equally probable intervals. Unlike traditional random sampling, LHS reduces the number of simulations needed while maintaining accuracy in estimating outcomes. This makes it particularly valuable in complex computational experiments. LHS ensures that there are no significant correlations between variables through utilizing a stochastic optimization method in which the difference between the initial and final correlation matrices can be minimized by the permutation of elements of the variables sample matrix.

By employing LHS, the generated dataset becomes a highly representative sample of the material characteristics within the input space. This ensures that the subsequent training of the machine learning model in the framework will be based on a comprehensive and accurate representation of the underlying data. This, in turn, enhances the model's ability to make reliable predictions and analyses.

After that, a Finite Element (FE) model of the composite is constructed, and multiple FE analyses are conducted to obtain the corresponding maximum stress of each composite candidate of the input space obtained from the generated LHS samples. Each sample has unique material properties for the most influential ply. It is a common practice to consider the top layer as the most influential ply (as indicated before) since it resists the highest normal straining actions during the bending of the entire composite.

At the end of this stage, the training dataset required for the next stage is ready. The input features (input design variables) of the dataset are the material characteristics (E_1, E_2, G_{12}, G_{23}, ν_{12}) of the most influential ply material; and the output is the maximum stress (the response quantity of interest).

Stage 3, Machine learning model training:

In the subsequent stage, the focus shifts to training a machine learning model. This process involves several steps:

Preparing the Dataset: This step involves organizing the data collected from the previous stage into a format suitable for training the machine learning model. It ensures that the input features (material characteristics) and the corresponding output (strength) are appropriately structured.

Dataset Normalization: Normalization is a crucial preprocessing step. It involves scaling the input features to a similar range, typically between 0 and 1. This ensures that all features contribute proportionally to the model's learning process, preventing any single variable from dominating the learning process due to differences in scale.

Random Splitting of Dataset: The dataset is divided into two subsets: a training set (70 %) and a testing set (30 %). The training set is used to train the model, while the testing set is reserved for evaluating its performance. Random splitting ensures that the two subsets are representative of the overall dataset and helps prevent overfitting.

Using the Dataset for training XGBoost model: XGBoost is a powerful machine-learning algorithm particularly suited for regression tasks [56]. XGBoost is an ensemble learning algorithm that combines the predictions of multiple decision trees. It is known for its high predictive accuracy and computational efficiency. It works by sequentially training an ensemble of weak learners (typically decision trees) and combining their predictions. The objective function $\mathscr{L}(\theta)$ to be minimized by XGBoost is as follows:

$$\mathscr{L}(\theta) = \sum_{i=1}^{n} l(\mathscr{Y}_i, \widehat{\mathscr{Y}}_i) + \sum_{i=1}^{k} \Omega(f_i) \tag{1}$$

Where n is the number of training examples, k is the number of trees in the ensemble, $\mathscr{Y}_i$ is the true output for the i-th example, $\widehat{\mathscr{Y}}_i$ is the predicted output for the i-th example, l is the loss function that measures the difference between true and predicted values, $\Omega(f_i)$ is the regularization term that penalizes the complexity of each tree.

The loss function l, which measures the squared difference between the true and predicted strength values is given as follows:

$$l(\mathscr{Y}_i, \widehat{\mathscr{Y}}_i) = (\mathscr{Y}_i - \widehat{\mathscr{Y}}_i)^2 \tag{2}$$

The regularization term $\Omega(f_i)$ discourages overfitting by penalizing complex trees and is given by:

$$\Omega(f_i) = \gamma T + \frac{1}{2}\lambda \sum_{j=1}^{T} w_j^2 \tag{3}$$

Where T is the number of leaves in the tree f_i, w_j are the weights associated with the leaves, γ and λ are hyperparameters controlling the strength of the regularization.

During training, XGBoost calculates the first and second derivatives of the loss function with respect to the predicted values. These are referred to as the gradient (g_i) and the Hessian (h_i):

$$g_i = \frac{\partial}{\partial \widehat{\mathscr{Y}}_i} l(\mathscr{Y}_i, \widehat{\mathscr{Y}}_i) \tag{4}$$

$$h_i = \frac{\partial^2}{\partial (\widehat{\mathscr{Y}}_i)^2} l(\mathscr{Y}_i, \widehat{\mathscr{Y}}_i) \tag{5}$$

and these quantities guide the optimization process. By optimizing the objective function using techniques like gradient boosting, XGBoost efficiently constructs an ensemble of trees that collectively provide accurate predictions for the strength of based on the main input parameters. In addition, the regularization terms ensure that the model remains robust and avoids overfitting.

Stage 4, XAI techniques to highlight the most important design parameters:

In this stage, the most important input features affecting the strength of the composite (the output response quantity) are investigated using SHapley Additive exPlanations (SHAP) technique and Partial dependence plots (PDPs).

SHAP is a mathematical technique based on game theory to describe the performance of a machine-learning model. It offers a profound understanding of the influence and significance of each input feature (E_1, E_2, G_{12}, G_{23}, ν_{12}) on the resulting composite strength. Furthermore, SHAP shows whether a feature positively or negatively impacts the composite's strength. This knowledge is pivotal for designers in pinpointing the most influential design variables that predominantly affect composite strength. It not only offers a global perspective on how input features affect the model, but also equips designers with a strategic approach to selecting and manipulating key parameters to exert a substantial impact on composite strength.

The mathematical representation of a Shapley value (ϕ_i) for a feature (x_i) in a cooperative game is defined as the average marginal contribution of that feature across all possible coalitions [57]:

$$\phi_i(f) = \sum_{S\subseteq N\backslash\{i\}} \frac{|S|! \bullet (|N| - |S| - 1)!}{|N|!} [f(S \cup \{i\}) - f(S)] \quad 6$$

Where N is the set of all features, S is a coalition of features that does not contain x_i, $f(S)$ is the model's prediction when considering only the features in S, $f(S \cup \{i\})$ is the model's prediction when adding x_i to S.

SHAP values provide a way to allocate the contribution of each input feature to the final prediction. They offer insights into the impact of individual features on a specific prediction. Positive SHAP values indicate a feature's positive contribution, while negative values indicate a negative contribution. This provides valuable insights for model interpretability and decision support that is highly required for the design process of the composite.

Contrarily, while SHAP excels at quantifying feature importance, it lacks the visual clarity of direct input–output relationships and struggles with identifying critical thresholds. To address these limitations, our proposed framework integrates Partial Dependence Plots (PDPs) alongside SHAP. PDPs provide an intuitive graphical overview of how individual features influence the response, facilitating straightforward interpretation and revealing interactions between features. They also offer insights into feature importance trends across their entire range and allow for efficient model comparison. This ensures a more comprehensive understanding of the model's behavior.

In PDP, a graphical relationship between a specific input feature and the output of a machine learning model is established while keeping all other features constant. They provide valuable insights into how changes in a single variable influence the model's predictions. Mathematically, PDP for a single input feature (x_i) can be expressed as follows [58]:

$$PDP(x_i) = \frac{1}{N}\sum_{j=1}^{N} f(x_{-i}, x_i^j) \quad 7$$

Where x_i is input feature of interest (one of material characteristics (E_1, E_2, G_{12}, G_{23}, ν_{12})), x_{-i} represents all the other features except x_i, x_i^j denotes the j-th value of feature x_i in the dataset, N is the total number of instances in the dataset, $f(x)$ is the machine learning model's prediction function.

The $PDP(x_i)$ at a given point x_i is computed by averaging the model's predicitions $f(x_{-i}, x_i^j)$ over all instances in the dataset, while keeping the feature x_i fixed at x_i^j.

By employing SHAP and PDPs, designers gain a valuable tool for understanding the individual effects of features on the model's predictions, aiding in model interpretation and decision-making. By the end of this stage, the designer will have a valuable insight on what are the impact of the each of material input parameters (E_1, E_2, G_{12}, G_{23}, ν_{12}) on the strength of the composite and which input parameter has the most dominant effect. But there is no information about how much change is required to happen in this dominant input feature to increase the composite strength to the required level. This is what will be discussed in the next stage.

Stage 5, Design stage using Counterfactual technique:

In this stage, the values of the crucial features identified in the preceding stage are adjusted to attain the desired strength for the composite. This is achieved by using the Counterfactual (CF) technique. Counterfactuals are hypothetical scenarios that represent what might have happened if a different set of conditions or actions were in place (i.e., changing the value of one of the input features). In the context of machine learning, counterfactual explanations provide insights into how changes in input features would have altered the model's prediction.

Let's assume that the following loss function needs minimizing [59,60]:

$$L(x, x', y', \lambda) = \lambda \bullet (\hat{f}(x') - y')^2 + d(x, x') \quad 8$$

The initial component (in the right-hand side) represents the quadratic discrepancy between the model's forecast for the counterfactual x', which is $\hat{f}(x')$, and the specified target y', as predetermined by the designer. The parameter λ balances the distance in prediction (first term) against the distance in feature values (second term). The subsequent component, denoted as d, quantifies the separation between the instance x under examination and the counterfactual x' (one of the input parameters). This loss function gauges both the deviation of the projected counterfactual outcome from the predefined target and the proximity of the counterfactual to the pertinent instance. The distance metric d is characterized as the Manhattan distance, with weighting factors determined by the inverse Median Absolute Deviation (MAD) for each feature, which can be represented as,$d(x, x') = \sum_{j=1}^{p} \frac{|x_j - x_j'|}{MAD_j}$

The overall distance is computed as the aggregate of p individual feature-wise distances, representing the absolute disparities in feature values between the given instance x and the counterfactual x'. These feature-specific distances are normalized by the reciprocal of the median absolute deviation (MAD) for feature j across the dataset, as stipulated by the formula:

$$MAD_j = \text{median}_{i\in\{1,\cdots,n\}}\left(|x_{i,j} - \text{median}_{l\in\{1,\cdots,n\}}(x_{l,j})|\right) \quad 9$$

The median of a vector marks the point at which half of the values are higher and the remaining half are lower. In contrast to the variance, MAD focuses on absolute differences, utilizing the median as the central measure. This method proves more resilient to outliers compared to the traditional Euclidean distance. The scaling operation with MAD is essential for standardizing features, ensuring consistency regardless of the measurement units.

The loss function is determined by a given parameter λ and yields a counterfactual x'. A higher λ indicates a preference for counterfactuals with predictions closely aligned to the desired outcome y', whereas a lower λ indicates a preference for counterfactuals x' that closely resemble the original instance x in terms of feature values. In cases where λ is exceedingly large, the instance with the prediction nearest to y' is selected, regardless of its distance from x. Ultimately, it falls upon the user to strike a balance between the requirement for the counterfactual's prediction to match the desired outcome (composite strength) and the requirement for the counterfactual to be similar to x. As an alternative to selecting a value for λ, a tolerance ε to specify how much deviation from y' (i.e., from the required strength) is permissible for the prediction of the counterfactual instance. This constraint can be represented as: $|\hat{f}(x') - y'| \leq \epsilon$.

To minimize this loss function, various optimization algorithms can be employed, including methods like Nelder-Mead for cases without gradient information. If gradients of the machine learning model are available, more efficient gradient-based methods like ADAM can be utilized (which is used in the current study). Prior to the optimization process, the instance x (the input features of interest) to be explained, the desired output y' (composite strength), and the predefined tolerance parameter ε (tolerance from the desired strength by the designer) must be specified. The loss function is iteratively minimized for x', gradually increasing the λ parameter, until a sufficiently close solution is achieved, falling within the specified tolerance limit: $\arg \min_{x'} \max_{\lambda} L(x, x', y', \lambda)$

In summary, the algorithm for generating counterfactuals can be summarized as follows:

1. Choose the instance x to be explained (all material input parameters (E_1, E_2, G_{12}, G_{23}, ν_{12})), specify the desired outcome y' (composite strength), set a tolerance level ε (the difference between the required strength and the actual strength), and initialize λ with a low value.
2. Begin with an initial counterfactual obtained by randomly sampling an instance.
3. Optimize the loss function, starting from this initial counterfactual.
4. While $|\widehat{f}(x') - y'| \leq \epsilon$, do the following:
   a. Increase λ.
   b. Optimize the loss function using the current counterfactual as the starting point.
   c. Select the counterfactual that minimizes the loss.
5. Iterate through steps 2 to 4 and return the counterfactual that achieves the lowest loss.

It worth mentioning here that XAI techniques offer notable advantages over common statistical methods like, for example, Response Surface Method (RSM). While RSM typically relies on fitting experimental data to polynomial models [61,62], often at the second level, XAI methods, such as counterfactuals, provide greater flexibility in capturing complex relationships without rigid assumptions about data distribution. Unlike RSM, which may face limitations in testing model suitability when the number of variables equals the number of experiments [63], XAI models excel in handling high-dimensional data and can offer insights even in scenarios with numerous variables. Additionally, while RSM may be susceptible to underfitting and struggle to capture intricate features of the response surface [62], XAI models aim to capture both global and local patterns, thereby mitigating underfitting and offering more comprehensive insights.

3. Validation of the proposed framework

The framework is validated using existing literature related to bridge decks [64]. FRP bridge decks are composed of upper and lower facesheets and sinusoidal core. The FRP decks shown in Fig. 3, which are often referred to as sandwich panels, are subjected to bending load in the direction of the loading, with negligible forces acting in the transverse direction (opposite to the traffic direction).

3.1. Finite Element (FE) model validation

Chen and Davalos [64] carried out a parametric study using experimental testing and FE analysis to optimize a selection of several laminates for the honeycomb sandwich panel's facesheet. The authors listed five different materials; material properties are shown in Table 1, and strength properties are shown in Table 2. The five materials are optimized into three laminates: 1, 2, and 3. Laminate 1 was considered unbalanced and tested in both longitudinal (L) and transverse (T) directions, while laminates 2 and 3 were balanced and only tested in one direction.

Table 1
Material properties for different plies [64].

Ply name	Commercial name	E_1 (GPa)	E_2 (GPa)	G_{12} (GPa)	G_{23} (GPa)	ν_{12}	ν_{23}
M1	CM 3205 UD	27.75	8.00	3.08	2.88	0.295	0.39
M2	CM 3205 CSM	11.79	11.79	4.21	2.36	0.402	0.4
M3	UM 1810 UD	30.06	8.55	3.30	3.08	0.293	0.386
M4	UM 1810 CSM	15.93	15.93	5.65	2.96	0.409	0.388
M5	Bond layer CSM	9.72	9.72	3.50	2.12	0.394	0.401

UD: Unidirectional, CSM: Chopped strand mat.

Table 2
Strength properties for different plies (MPa) [64].

Ply name	X_T	X_C	Y_T	Y_C	S_{12}	S_{23}
M1	1341	404	46	66	46	46
M2	152	152	152	152	76	83
M3	1452	409	46	65	46	46
M4	159	159	159	159	79	83
M5	147	147	147	147	73	83

X_T: longitudinal tensile failure stress, X_C: longitudinal compressive failure stress, Y_T: transversal tensile failure stress, Y_C: transversal compressive failure stress, S_{12}: axial failure stress, and S_{23}: transverse failure stress.

For validation purposes, a Finite Element model is constructed using commercial software ABAQUS [66]. Shell elements (S4R) are used to construct a 381 mm length by 50.8 mm width plate subjected to three-point bending with a 305 mm span. For each material, elastic properties are assigned according to Table 1, while strength parameters, shown in Table 2, are defined as a part of Hashin damage in ABAQUS. Hashin damage contains strength parameters, damage evolution, and damage stabilization to avoid convergence problems. In this model, an energy-softening damage type is selected. Longitudinal tensile and compressive fracture energy are assumed 40 N/mm, while transverse tensile and compressive fracture energy are assumed 4 N/mm. The viscosity parameter for the damage stabilization is assumed to be 0.0001. The stacking sequence followed the laminates 1, 2, and 3 presented in the literature [64].

The FE results shown in Fig. 4 show a good correlation between the FE results and experimental results (especially for the maximum

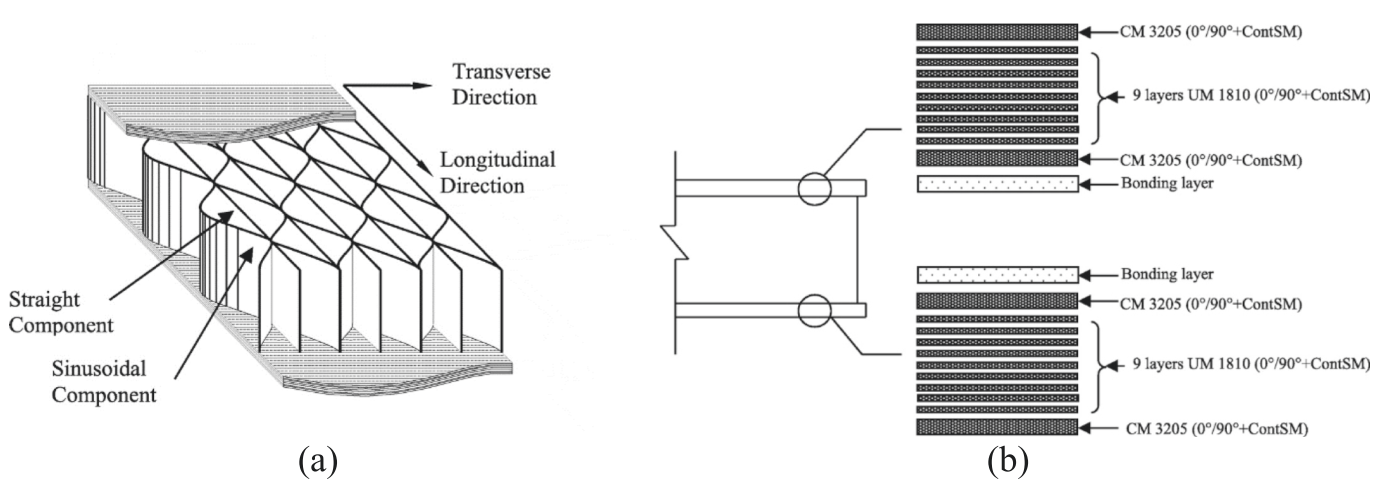

Fig. 3. Sketch showing (a) FRP bridge deck components and (b) stacking sequence of facesheets laminates [65].

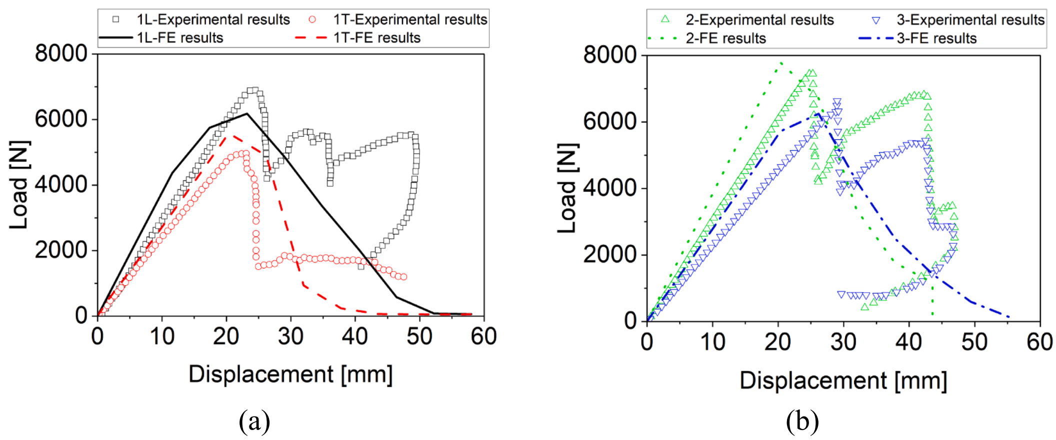

Fig. 4. Validation of FE results versus experimental results for (a) laminate 1 and (b) laminates 2 and 3.

strength) for the three laminates. Therefore, the FE model is used for further analysis.

3.2. Stacking sequence optimization

In this study, maximum strength is selected as an objective function output. The number of the plies is reduced to 14 plies with a symmetric configuration. The brute force optimization is performed by employing a Python script within ABAQUS CAE module to change the stacking arrangement of the top 7 plies according to the available 5 materials while avoiding repeating the same material consecutively.

The optimization is carried out using High Performance Computing (HPC) (CSC, Finland) on 1 CPU node with two Intel Xeon processors, where each includes 20 cores running at 2.1 GHz. The optimization yields to global optimal strength of 809 MPa, and the stacking arrangement is [M1, M5, M1, M3, M5, M2, M5]. Based on the optimization result, M1 is selected as the most influential ply material as it is placed at the top layer.

3.3. Dataset generation

Dataset generation is performed using the design of experiments. The number of samples is reduced from 3000 samples to 1000 samples and distributed using Latin Hypercube Sampling (LHS). The higher and lower bounds for each material property (i.e., E_1, E_2, etc.) are selected as a sampling boundary based on Table 1 while satisfying the constraints that stiffness in the longitudinal direction is larger or equal than the transversal direction. The generated data from LHS are used as input data for FE analysis.

To run the FE analysis, first, the material parameters for material M1 are modified according to the LHS-generated data. It is worth noting that the material M1 is reflected in four plies out of 14 plies, including the most top and bottom plies. ABAQUS input files for the 1000 samples are first created, and then each 200 input files are run simultaneously on HPC. After the analysis, the maximum mises stress is extracted for the samples. Fig. 5 shows a stress output for one of the configurations.

3.4. Machine learning training

The generated data from LHS are used as input data for training with input parameters defined as (E_1, E_2, G_{12}, G_{23}, ν_{12}). The output parameter for the ML training is assigned as maximum stress. The data is trained using XGBoost Random Forest Regressor, yielding to mean R^2 value of 0.95 which falls within acceptable prediction region. Fig. 6 shows the residuals and prediction errors plots of the XGBoost Random Forest Regressor.

Fig. 7 shows the histograms of the generated data set. Each histogram represents the frequency distribution of a single feature. The x-axis of each histogram represents the range of values for the feature, and the y-axis represents the number of data points that fall within each range. Histograms shows that the LHS has successfully distributed the input parameters across the bounds.

3.5. Explainable Machine learning (XAI)

The input and output parameters are further analyzed using partial dependence plot (PDP) and SHapley Additive exPlanations (SHAP) [67]. Fig. 8 shows the PDP plots for the input parameters, which illustrates the

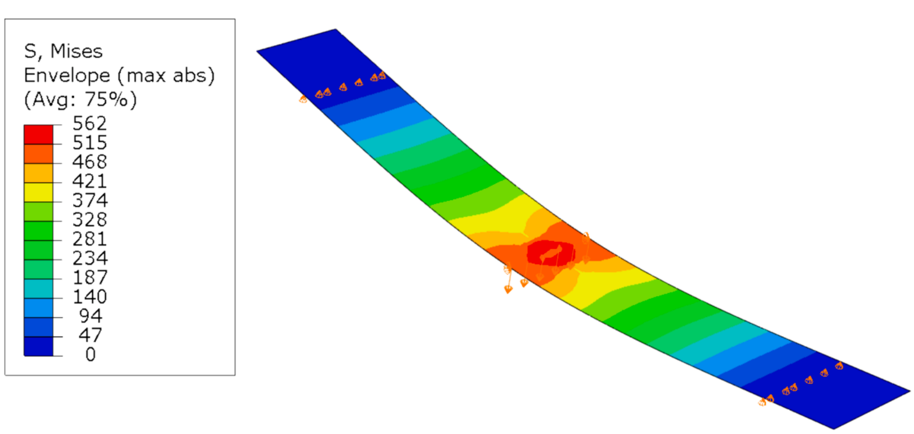

Fig. 5. FE model of facesheet subjected to flexural loading.

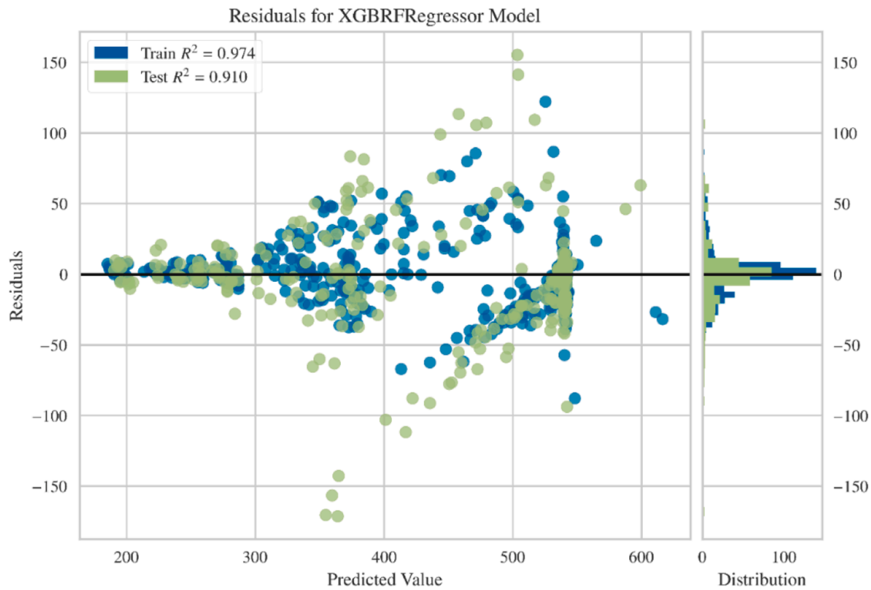

a. Residuals plot of the XGBoost model

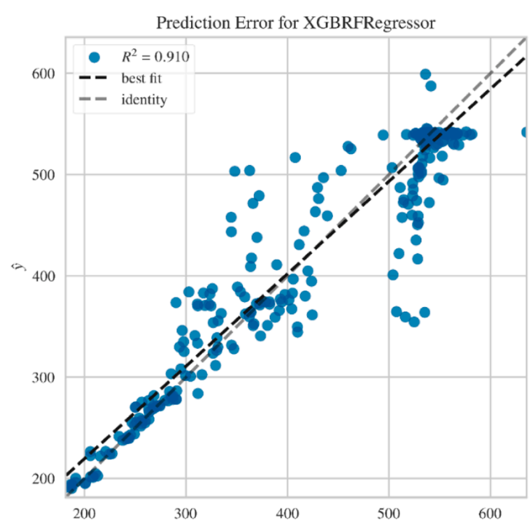

b. Prediction error plot of the XGBoost model

Fig. 6. Accuracy of the XGBoost model.

correlation between the partial dependency of the average response parameter and the variations in the input feature values. The plots show that the variation in E_1 from 12500 MPa to 22500 MPa will result in a direct change in the output strength. Increasing E_1 beyond 22,500 will result in insignificant changes in the output strength. The other input parameters are showing a limited partial dependence which implies that they have marginal effect on the output strength.

Fig. 9 shows the SHAP value for each input parameter. As shown, E_1 has the highest impact on the overall behavior of the strength. The red region, which indicates the high impact of the input parameter for E_1 is located on the positive side, which implies that the E_1 is directly proportional to the output strength. Other input parameters are located around SHAP value of zero, which agrees with the PDP results as E_1 directly impact the flexural stress results. Based on the XAI models (i.e., PDP and SHAP), we can conclude that the E_1 is the most important parameter.

Fig. 10 is a correlation matrix visualization, where each cell represents the correlation coefficient between two features from the dataset. The correlation coefficient is a statistical measure that indicates the strength and direction of the linear relationship between two variables. It ranges from −1 to 1, where: "1″ indicates a perfect positive correlation, meaning as one variable increases, the other variable also increases proportionally. "-1" indicates a perfect negative correlation, meaning as one variable increases, the other variable decreases proportionally. "0" indicates no linear correlation between the variables. The figure shows that there is a strong positive correlation between E_1 and stress (0.89), and weaker correlation between E_1 and E_2 (0.19) and E_2 and stress (0.19). Correlation (by heatmap) does not imply causation. In other words, if two features are correlated does not necessarily mean that one causes the other. The heatmap only shows linear correlations. It is possible for features to have non-linear relationships that are not captured by the correlation coefficient.

The correlation in the heat map has successfully indicated that stress relays mostly in E_1, which correlates well with the design of the experiment where the laminate is subjected to bending which translates into longitudinal stresses. Therefore, based on the engineering designers

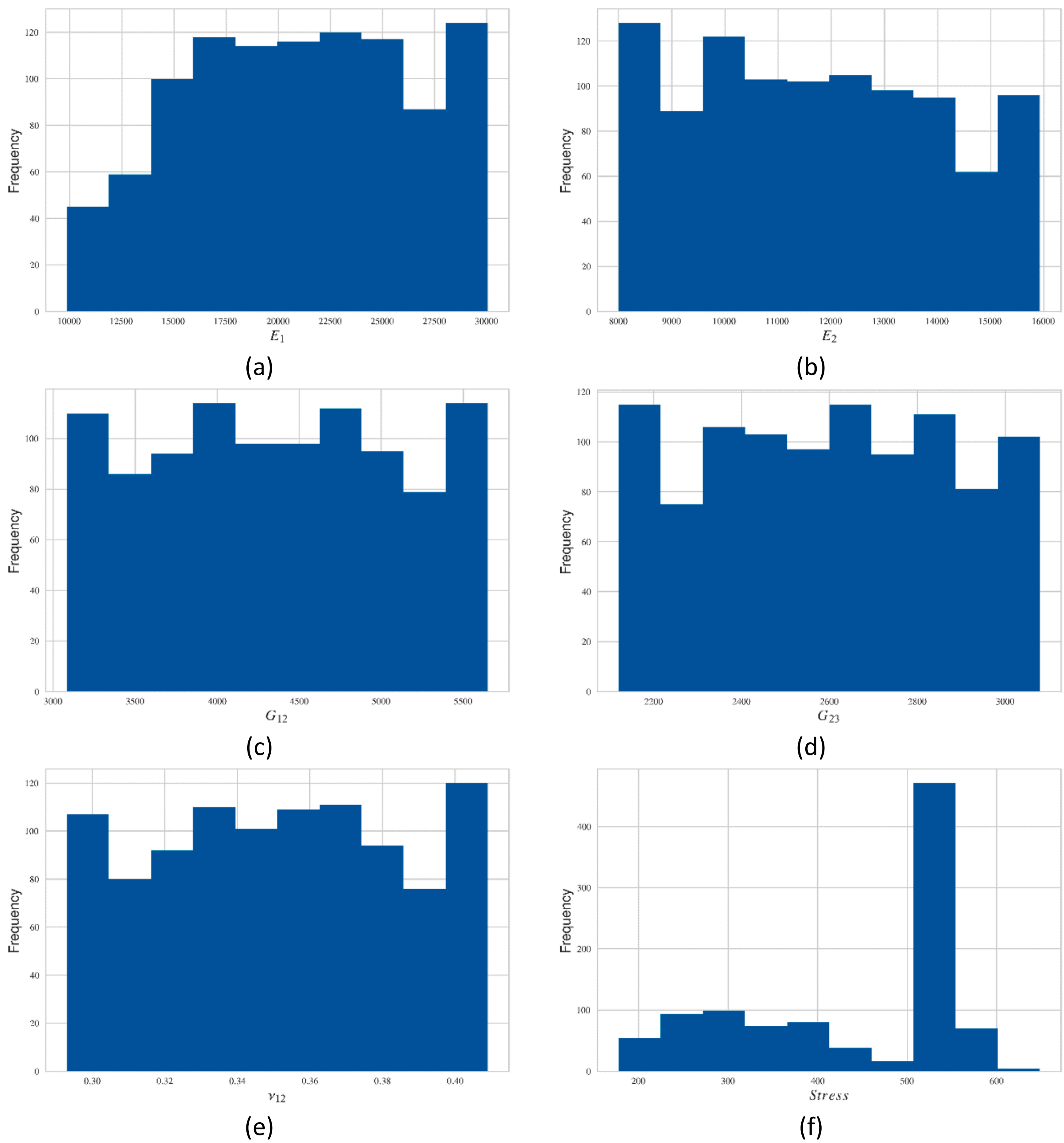

Fig. 7. Histograms for (a) E_1, (b) E_2, (c) G_{12}, (d) G_{23}, (e) ν_{12} and (f) stress.

intuition, stress is expected to depend on E_1 more than any other input, which is pointed out from the heat map. However, it worth mentioning that heat map does not provide the relation between the inputs and output neither it provides the amount of change needed for to achieve the desired output space.

3.6. Design stage using counterfactual (CF)

After knowing the most important design parameters affecting the composite strength from section 3.5, the next step is to adjust these parameters to achieve the desired composite strength. Adjusting the design parameters will be conducted in this section through the Counterfactual (CF) technique. Based on SHAP and PDP plots explained in the previous section, E_1 is found the most influential design parameters. So, the main change will be in E_1 while other parameters will be affected by this change in E_1 because of the inherent correlation among the input features as shown in the heat map plot in the previous section. Designing using CF is performed by defining the Current State (CS) stress and the desired design range. It worth mentioning that for generating the counterfactuals, the same algorithm explained in stage 5 (under section 2) is used. The desired outcome y' (composite strength) is a class range of 600 MPa and 800 MPa. The tolerance level ε (the difference between the

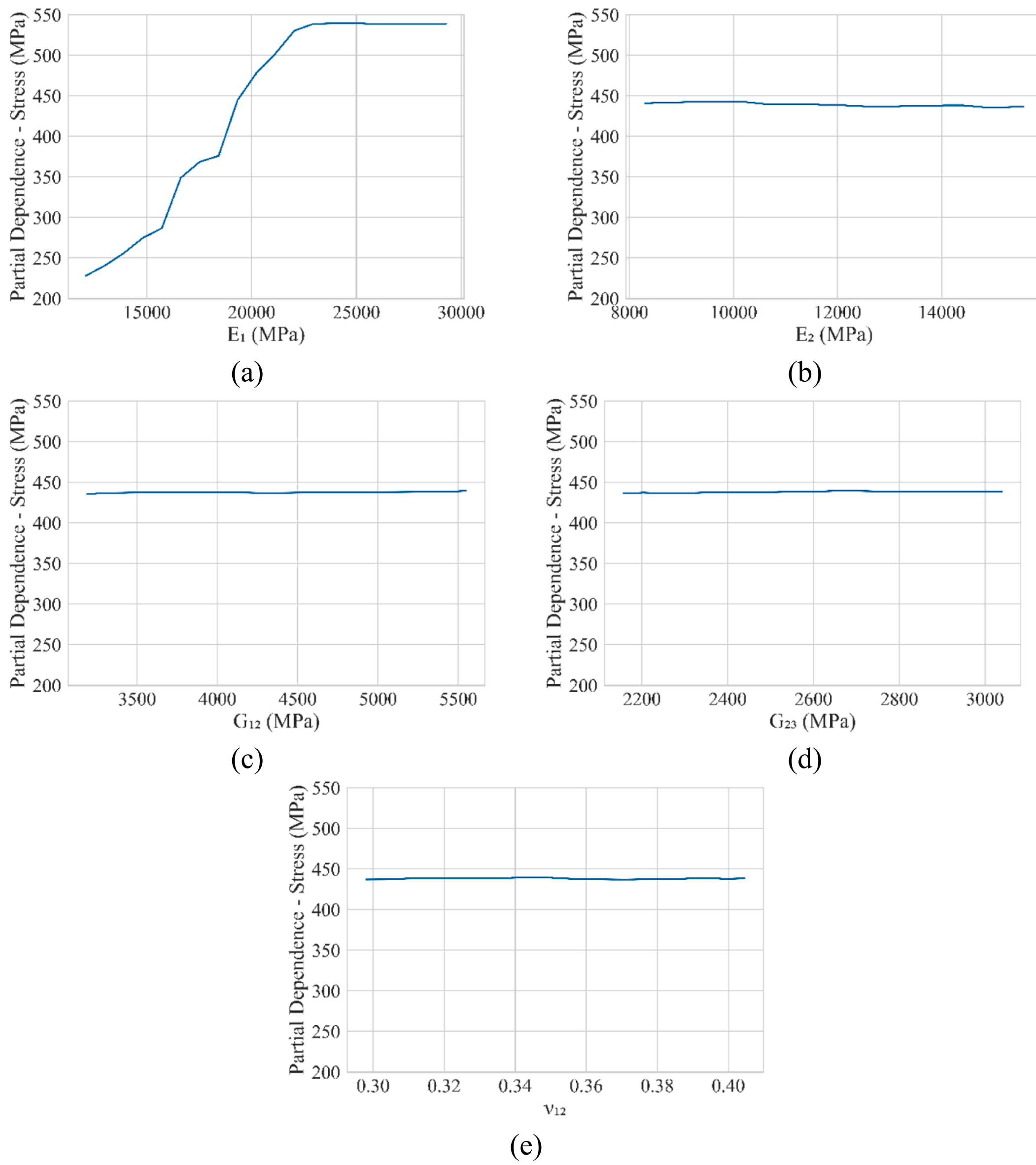

Fig. 8. PD plots for (a) E_1, (b) E_2, (c) G_{12}, (d) G_{23}, (e) ν_{12}.

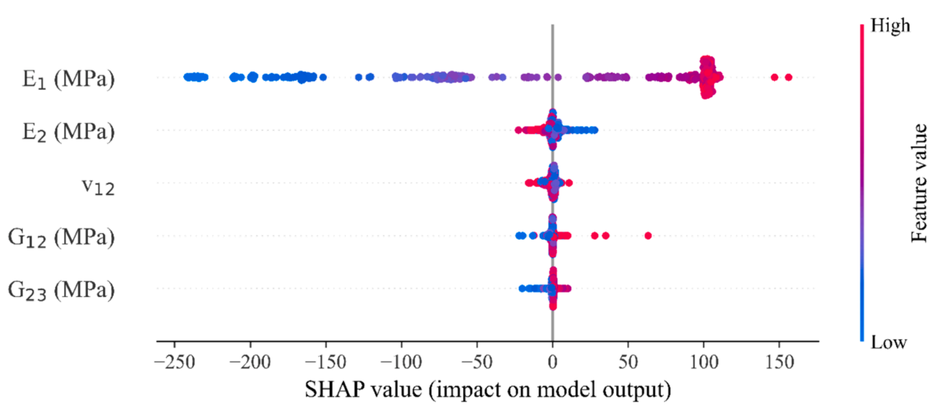

Fig. 9. SHAP plot for different input parameters.

required strength and the actual strength) is set to approximately 5 %. The initial counterfactual is the original value of E_1 in the instance selected for design. In this study, the current state is varied depending on any configuration, while the design stress range is defined between 600 MPa and 800 MPa, which represents the highest 25 % of the brute force optimization results. Two examples are shown in Table 3, showing the

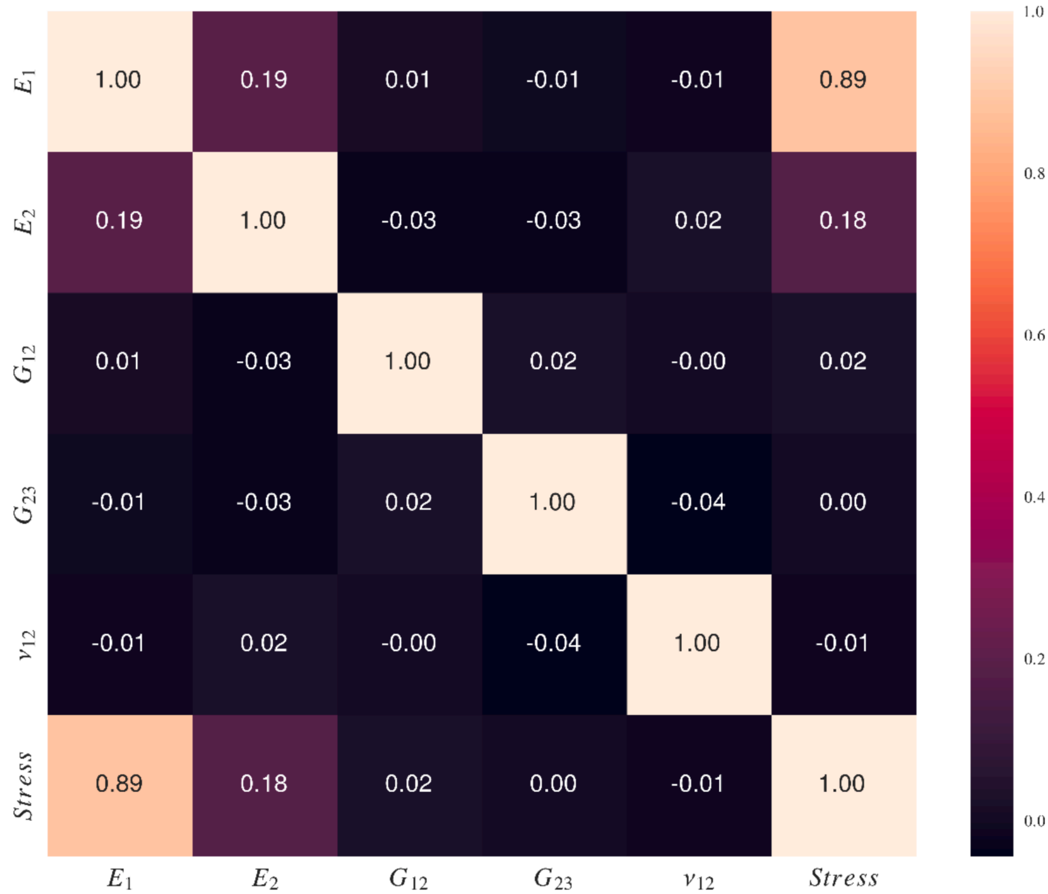

Fig. 10. Heat map of the correlation among all features of the dataset.

Table 3
Different values for Current and Design States.

State	E_1 (MPa)	E_2 (MPa)	G_{12} (MPa)	G_{23} (MPa)	ν_{12}	Stress (MPa)*
Current State 1	29,703	11,031	3434	2896	0.336	554.7
Design State 1A	30,018	8570	3284	2618	0.342	642.8
Design State 1B	30,032	14,754	4204	2730	0.326	625.2
Current State 2	12,720	8488	4245	2878	0.384	255.1
Design State 2A	29,990	12,338	4435	2772	0.384	631.7
Design State 2B	30,018	8001	3284	2635	0.384	636.1

* The results obtained are found to have discrepancy less than 3% compared to FE analysis results.

current state and the design states suggested by the CF model. In the first case, the first option suggests that E_1 should increase from 29703 MPa to 30018 MPa to increase the output stress from 554.7 MPa to 642.8 MPa, while the second option proposes that E_1, E_2, and G_{12} increase to increase the stress to 625.2 MPa, as shown in the table. Based on suggested options, the engineer can then choose which option fits the available plies. Another case is presented, showing similar results to the first case, where E_1 is the dominant input parameter. Generating these results took, on average, 1 min on a desktop computer with Intel Xeon 8 cores, which shows that using the CF can ultimately enhance the design process and significantly reduce the computational cost compared to traditional design methods and FE analysis.

4. Conclusions

An explainable artificial intelligence (XAI) technique is used for the first time as a design tool for composite design. Stacking sequence is varied using brute force optimization to achieve global output strength for laminate. Based on optimization results and expert view, a selection for the most important ply material is further analyzed. The ply material properties are distributed using Latin Hypercube Sampling (LHS) to generate input parameters and output strength is predicted using Finite Element (FE) analysis. The ply material properties are distributed using LHS to generate a representative sample of the entire input space. FE analyses are conducted to calculate output strengths of samples. The input and output parameters are further used to train a machine learning (ML) model and the interpretability of the model is further investigated using XAI to highlight the most influential input features on the composite strength. The testing and training accuracies of the ML model reached 91.02 %, and 97.44 %, respectively, indicating its ability to predict outcomes with high precision. The results showed that the longitudinal modulus of the ply material (E_1) has a dominant effect on the composite strength compared to other input features.

After that, a counterfactual (CF) technique is used as a design tool to adjust values of the input features to obtain the required composite strength. It is found that the CF technique can provide the design values of the input features to obtain the required composite strength. As an example, to elevate the output strength from 554.7 MPa to 642.8 MPa, a targeted increase in the E_1 value, from 29703 MPa to 30018 MPa, is necessary. The strength results of the CF techniques founded to be in a very good agreement of those obtained using FE analysis for the same tested samples. Based on these results, employing the proposed framework will empower designers to efficiently pinpoint the most direct route to attain the desired composite design, leading to substantial reductions in computational expenses and streamlining the lamina selection process.

However, this study acknowledges certain limitations, such as the need for further validation across diverse composite configurations and material systems. Additionally, while the proposed framework demonstrates promise in streamlining design processes and reducing computational burdens, its applicability to real-world scenarios warrants additional investigation.

Looking ahead, future research avenues may include refining XAI techniques for deeper insights into complex material behaviors, exploring alternative optimization algorithms to enhance efficiency, and extending the framework to account for multi-objective optimization objectives. Ultimately, the proposed methodology holds substantial potential to empower designers with efficient tools for achieving optimal composite designs, thereby facilitating advancements in various engineering applications.

CRediT authorship contribution statement

Mostafa Yossef: Data curation. **Mohamed Noureldin:** Writing – review & editing, Writing – original draft, Conceptualization. **Aghyad Alqabbany:** Validation, Software, Methodology.

Declaration of competing interest

The authors declare that they have no known competing financial interests or personal relationships that could have appeared to influence the work reported in this paper.

Data availability

Data will be made available on request.

Acknowledgments

Mostafa Yossef would like to acknowledge the Research Council of Finland for the academy postdoctoral fellowship grant no. 348611. The authors wish to acknowledge CSC – IT Center for Science, Finland, for computational resources.

References

[1] Xie H, Shen C, Fang H, Han J, Cai W. Flexural property evaluation of web reinforced GFRP-PET foam sandwich panel: Experimental study and numerical simulation. Compos B Eng 2022;234:109725. https://doi.org/10.1016/j.compositesb.2022.109725.
[2] Yossef M, Chen A, Downey A. Development of a photovoltaic integrated insulated concrete sandwich panel. ACI Special Publication 2018;327:29.1–29.18.
[3] Yossef M, Chen A. A solution considering partial degree of composite action for insulated sandwich panels with general configuration flexible shear connectors. Eng Struct 2018;162:135–50. https://doi.org/10.1016/j.engstruct.2018.02.019.
[4] Chen A, Yossef M, Hopkins P. A comparative study of different methods to calculate degrees of composite action for insulated concrete sandwich panels. Eng Struct 2020;212:110423. https://doi.org/10.1016/j.engstruct.2020.110423.
[5] Hopkins PM, Chen A, Yossef M. Static and dynamic analyses of insulated concrete sandwich panels using a unified non-linear finite element model. Eng Struct 2017:132. https://doi.org/10.1016/j.engstruct.2016.11.017.
[6] Shen M-Y, Guo Z-H, Feng W-T. A study on the characteristics and thermal properties of modified regenerated carbon fiber reinforced thermoplastic composite recycled from waste wind turbine blade spar. Compos B Eng 2023;264:110878. https://doi.org/10.1016/j.compositesb.2023.110878.
[7] Özkan R, Genç MS. Aerodynamic design and optimization of a small-scale wind turbine blade using a novel artificial bee colony algorithm based on blade element momentum (ABC-BEM) theory. Energy Convers Manag 2023;283:116937. https://doi.org/10.1016/j.enconman.2023.116937.
[8] Guangxing G, Weijun Z, Zhenye S, Wenzhong S, Jiufa C, Shifeng F. Drag reducer design of wind turbine blade under flap-wise fatigue testing. Compos Struct 2023;318:117094. https://doi.org/10.1016/j.compstruct.2023.117094.
[9] Tran P, Nguyen QT, Lau KT. Fire performance of polymer-based composites for maritime infrastructure. Compos B Eng 2018;155:31–48. https://doi.org/10.1016/j.compositesb.2018.06.037.
[10] Robin A, Arhant M, Davies P, Lejeune S, Lolive E, Bonnemains T, et al. Effect of aging on the in-plane and out-of-plane mechanical properties of composites for design of marine structures. Composites Part C: Open Access 2023;11:100354. https://doi.org/10.1016/j.jcomc.2023.100354.
[11] Pacheco-Blazquez R, Di Capua D, García-Espinosa J, Casals O. Methodology and application to assess thermo-mechanical buckling in composite marine structures. Ocean Eng 2023;267:113002. https://doi.org/10.1016/j.oceaneng.2022.113002.
[12] Tan W, Naya F, Yang L, Chang T, Falzon BG, Zhan L, et al. The role of interfacial properties on the intralaminar and interlaminar damage behaviour of unidirectional composite laminates: experimental characterization and multiscale modelling. Compos B Eng 2018;138:206–21. https://doi.org/10.1016/j.compositesb.2017.11.043.
[13] Badalló P, Trias D, Marín L, Mayugo JA. A comparative study of genetic algorithms for the multi-objective optimization of composite stringers under compression loads. Compos B Eng 2013;47:130–6. https://doi.org/10.1016/j.compositesb.2012.10.037.
[14] Noureldin M, Ali A, Memon S, Kim J. Fragility-based framework for optimal damper placement in low-rise moment-frame buildings using machine learning and genetic algorithm. J Build Eng 2022;54:104641. https://doi.org/10.1016/j.jobe.2022.104641.
[15] Ji H, Ye H. Machine learning prediction of corrosion rate of steel in carbonated cementitious mortars. Cem Concr Compos 2023;143:105256. https://doi.org/10.1016/j.cemconcomp.2023.105256.
[16] Li H-W-X, Lyngdoh G, Krishnan NMA, Das S. Machine learning guided design of microencapsulated phase change materials-incorporated concretes for enhanced freeze-thaw durability. Cem Concr Compos 2023;140:105090. https://doi.org/10.1016/j.cemconcomp.2023.105090.
[17] Sayed YAK, Ibrahim AA, Tamrazyan AG, Fahmy MFM. Machine-learning-based models versus design-oriented models for predicting the axial compressive load of FRP-confined rectangular RC columns. Eng Struct 2023;285:116030. https://doi.org/10.1016/j.engstruct.2023.116030.
[18] Zhang S, Xu J, Lai T, Yu Y, Xiong W. Bond stress estimation of profiled steel-concrete in steel reinforced concrete composite structures using ensemble machine learning approaches. Eng Struct 2023;294:116725. https://doi.org/10.1016/j.engstruct.2023.116725.
[19] Pallapothu SNRG, Pancharathi RK, Janib R. Predicting concrete strength through packing density using machine learning models. Eng Appl Artif Intel 2023;126:107177. https://doi.org/10.1016/j.engappai.2023.107177.
[20] Ali T, Eldin MN, Haider W. The effect of soil-structure interaction on the seismic response of structures using machine learning, finite element modeling and ASCE 7–16 methods. Sensors 2023;23:2047. https://doi.org/10.3390/s23042047.
[21] Pei Z, Rozman KA, Doğan ÖN, Wen Y, Gao N, Holm EA, et al. Machine-learning microstructure for inverse material design. Adv Sci 2021:8. https://doi.org/10.1002/advs.202101207.
[22] Hasan M, Acar P. Machine learning reinforced microstructure-sensitive prediction of material property closures. Comput Mater Sci 2022;210:110930. https://doi.org/10.1016/j.commatsci.2021.110930.
[23] Liu R, Kumar A, Chen Z, Agrawal A, Sundararaghavan V, Choudhary A. A predictive machine learning approach for microstructure optimization and materials design. Sci Rep 2015;5:11551. https://doi.org/10.1038/srep11551.
[24] Le T-T. Prediction of tensile strength of polymer carbon nanotube composites using practical machine learning method. J Compos Mater 2021;55:787–811. https://doi.org/10.1177/0021998320953540.
[25] Rahman A, Deshpande P, Radue MS, Odegard GM, Gowtham S, Ghosh S, et al. A machine learning framework for predicting the shear strength of carbon nanotube-polymer interfaces based on molecular dynamics simulation data. Compos Sci Technol 2021;207:108627. https://doi.org/10.1016/j.compscitech.2020.108627.
[26] Noureldin M, Gharagoz MM, Kim J. Seismic retrofit of steel structures with re-centering friction devices using genetic algorithm and artificial neural network. Steel Compos Struct 2023;47:167–84. https://doi.org/10.12989/scs.2023.47.2.167.
[27] Noureldin M, Ali A, Sim S, Kim J. A machine learning procedure for seismic qualitative assessment and design of structures considering safety and serviceability. J Build Eng 2022;50:104190. https://doi.org/10.1016/j.jobe.2022.104190.
[28] Noureldin M, Ali T, Kim J. Machine learning-based seismic assessment of framed structures with soil-structure interaction. Front Struct Civ Eng 2023;17:205–23. https://doi.org/10.1007/s11709-022-0909-y.
[29] Noureldin M, Ali A, Nasab MSE, Kim J. Optimum distribution of seismic energy dissipation devices using neural network and fuzzy inference system. Comput Aided Civ Inf Eng 2021;36:1306–21. https://doi.org/10.1111/mice.12673.
[30] Qiu C, Yang J. Machine learning applications in composites: manufacturing, design, and characterization. Comput Mater Sci 2022:65–85. https://doi.org/10.1021/bk-2022-1416.ch004.
[31] Qiu C, Han Y, Shanmugam L, Zhao Y, Dong S, Du S, et al. A deep learning-based composite design strategy for efficient selection of material and layup sequences from a given database. Compos Sci Technol 2022;230:109154. https://doi.org/10.1016/j.compscitech.2021.109154.
[32] Okafor CE, Iweriolor S, Ani OI, Ahmad S, Mehfuz S, Ekwueme GO, et al. Advances in machine learning-aided design of reinforced polymer composite and hybrid material systems. Hybrid Advances 2023;2:100026. https://doi.org/10.1016/j.hybadv.2023.100026.
[33] Li M, Zhang H, Li S, Zhu W, Ke Y. Machine learning and materials informatics approaches for predicting transverse mechanical properties of unidirectional CFRP composites with microvoids. Mater Des 2022;224. https://doi.org/10.1016/j.matdes.2022.111340.

[34] Liu B, Vu-Bac N, Rabczuk T. A stochastic multiscale method for the prediction of the thermal conductivity of polymer nanocomposites through hybrid machine learning algorithms. Compos Struct 2021;273:114269. https://doi.org/10.1016/j.compstruct.2021.114269.
[35] Liu X, Tian S, Tao F, Yu W. A review of artificial neural networks in the constitutive modeling of composite materials. Compos B Eng 2021;224:109152. https://doi.org/10.1016/j.compositesb.2021.109152.
[36] Li Z, Li X, Chen Y, Zhang C. A mechanics-informed machine learning approach for modeling the elastoplastic behavior of fiber-reinforced composites. Compos Struct 2023;323:117473. https://doi.org/10.1016/j.compstruct.2023.117473.
[37] Gu GX, Chen C-T, Buehler MJ. De novo composite design based on machine learning algorithm. Extreme Mech Lett 2018;18:19–28. https://doi.org/10.1016/j.eml.2017.10.001.
[38] Yang C, Kim Y, Ryu S, Gu GX. Prediction of composite microstructure stress-strain curves using convolutional neural networks. Mater Des 2020;189:108509. https://doi.org/10.1016/j.matdes.2020.108509.
[39] Mishra BB, Kumar A, Samui P, Roshni T. Buckling of laminated composite skew plate using FEM and machine learning methods. Engineering Computations (Swansea, Wales) 2021;38:501–28. https://doi.org/10.1108/EC-08-2019-0346.
[40] Furtado C, Pereira LF, Tavares RP, Salgado M, Otero F, Catalanotti G, et al. A methodology to generate design allowables of composite laminates using machine learning. Int J Solids Struct 2021;233:111095. https://doi.org/10.1016/j.ijsolstr.2021.111095.
[41] Oliveira GAB, Câmara ECB, Freire Júnior RCS. Obtaining G12 and Xt using mixed ANNs based on matrix and fiber properties. Compos B Eng 2019;175:107171. https://doi.org/10.1016/j.compositesb.2019.107171.
[42] Liu X, Liu T, Feng P. Long-term performance prediction framework based on XGBoost decision tree for pultruded FRP composites exposed to water, humidity and alkaline solution. Compos Struct 2022;284:115184. https://doi.org/10.1016/j.compstruct.2022.115184.
[43] Duan J, Asteris PG, Nguyen H, Bui X-N, Moayedi H. A novel artificial intelligence technique to predict compressive strength of recycled aggregate concrete using ICA-XGBoost model. Eng Comput 2021;37:3329–46. https://doi.org/10.1007/s00366-020-01003-0.
[44] Sharma A, Mukhopadhyay T, Rangappa SM, Siengchin S, Kushvaha V. Advances in computational intelligence of polymer composite materials: machine learning assisted modeling, analysis and design. Arch Comput Meth Eng 2022;29:3341–85. https://doi.org/10.1007/s11831-021-09700-9.
[45] Kibrete F, Trzepieciński T, Gebremedhen HS, Woldemichael DE. Artificial intelligence in predicting mechanical properties of composite materials. J Compos Sci 2023;7:364. https://doi.org/10.3390/jcs7090364.
[46] Das PP, Elenchezhian M, Vadlamudi V, Raihan R. Artificial Intelligence Assisted Residual Strength and Life Prediction of Fiber Reinforced Polymer Composites. AIAA SCITECH 2023 Forum, Reston, Virginia: American Institute of Aeronautics and Astronautics; 2023. https://doi.org/10.2514/6.2023-0773.
[47] Kulasooriya WKVJB, Ranasinghe RSS, Perera US, Thisovithan P, Ekanayake IU, Meddage DPP. Modeling strength characteristics of basalt fiber reinforced concrete using multiple explainable machine learning with a graphical user interface. Sci Rep 2023;13:13138. https://doi.org/10.1038/s41598-023-40513-x.
[48] Meister S, Wermes M, Stüve J, Groves RM. Investigations on explainable artificial intelligence methods for the deep learning classification of fibre layup defect in the automated composite manufacturing. Compos B Eng 2021;224:109160. https://doi.org/10.1016/j.compositesb.2021.109160.
[49] Saberi S, Nasiri H, Ghorbani O, Friswell MI, Castro SGP. Explainable artificial intelligence to investigate the contribution of design variables to the static characteristics of bistable composite laminates. Materials 2023;16. https://doi.org/10.3390/ma16155381.
[50] Chiu YH, Liao YH, Juang JY. Designing bioinspired composite structures via genetic algorithm and conditional variational autoencoder. Polymers (Basel) 2023;15. https://doi.org/10.3390/polym15020281.
[51] Zhao J, Wang B, Lyu Q, Xie W, Guo Z, Wang B. Compression after multiple impact strength of composite laminates prediction method based on machine learning approach. Aerosp Sci Technol 2023;136:108243. https://doi.org/10.1016/j.ast.2023.108243.
[52] Liang S, Shen Y, Ren X. Comparative study of influential factors for punching shear resistance/failure of RC slab-column joints using machine-learning models. Structures 2022;45:1333–49. https://doi.org/10.1016/j.istruc.2022.09.110.
[53] Bakouregui AS, Mohamed HM, Yahia A, Benmokrane B. Explainable extreme gradient boosting tree-based prediction of load-carrying capacity of FRP-RC columns. Eng Struct 2021;245. https://doi.org/10.1016/j.engstruct.2021.112836.
[54] Naser MZ. An engineer's guide to eXplainable artificial intelligence and interpretable machine learning: navigating causality, forced goodness, and the false perception of inference. Autom Constr 2021;129. https://doi.org/10.1016/j.autcon.2021.103821.
[55] Tsai SW. Double–double: new family of composite laminates. AIAA J 2021;59:4293–305. https://doi.org/10.2514/1.J060659.
[56] Chen T, Guestrin C. In: XGBoost. New York, NY, USA: ACM; 2016. p. 785–94. https://doi.org/10.1145/2939672.2939785.
[57] Lundberg S, Lee S-I. A Unified Approach to Interpreting Model Predictions. 31st Conference on Neural Information Processing Systems, Long Beach, CA, USA, 2017.
[58] Noureldin M, Abuhmed T, Saygi M, Kim J. Explainable probabilistic deep learning framework for seismic assessment of structures using distribution-free prediction intervals. Comput Aided Civ Inf Eng 2023;38:1677–98. https://doi.org/10.1111/mice.13015.
[59] Wachter S, Mittelstadt B, Russell C. Counterfactual explanations without opening the black box: automated decisions and the GDPR. Harv J Law Technol 2018;31:841–87.
[60] Molnar C. Interpretable machine learning. 2022.
[61] Aydar AY. Utilization of Response Surface Methodology in Optimization of Extraction of Plant Materials. In: Statistical Approaches With Emphasis on Design of Experiments Applied to Chemical Processes. InTech; 2018. https://doi.org/10.5772/intechopen.73690.
[62] Khuri AI, Cornell JA. Response surfaces: designs and analyses. CRC press; 2018. https://doi.org/10.1201/9780203740774.
[63] David Harvey. Using R to Model a Response Surface (Multiple Regression). Chemometrics Using R, DePauw University; 2021.
[64] Chen A, Davalos JF. Development of facesheet for honeycomb FRP sandwich panels. J Compos Mater 2012. https://doi.org/10.1177/0021998312437432.
[65] Chen A, Davalos JF. Design Equations and Example for FRP Deck–Steel Girder Bridge System. Practice Periodical on Structural Design and Construction 2014;19. https://doi.org/10.1061/(asce)sc.1943-5576.0000173.
[66] ABAQUS. ABAQUS Documentation 2022.
[67] Python 3.12 Contributors. Python 3.12 2023.